JCTC Journal of Chemical Theory and Computation

Article

Cite This: J. Chem. Theory Comput. 2019, 15, 2278−2290

pubs.acs.org/JCTC

A Combined Spin-Flip and IP/EA Approach for Handling Spin and Spatial Degeneracies: Application to Double Exchange Systems

Shannon E. Houck and Nicholas J. Mayhall*

Department of Chemistry, Virginia Tech, Blacksburg, Virginia 24060, United States

Supporting Information

ABSTRACT: Many multiconfigurational systems, such as single-molecule magnets, are difficult to study using traditional computational methods due to the simultaneous existence of both spin and spatial degeneracies. In this work, a new approach termed *n*-spin-flip ionization potential/electron affinity (*n*SF-IP or *n*SF-EA) is introduced which combines the spin-flip method of Anna Krylov with particle-number changing IP/EA methods. We demonstrate the efficacy of the approach by applying it to the strongly correlated N_2^+, as well as several double exchange systems. We also demonstrate that when these systems are well-described by a double exchange model Hamiltonian, only 1SF-IP/EA is required to extract the double exchange parameters and accurately predict energies for the low-spin states. This significantly reduces the computational effort for studying such systems. The effects of including additional excitations (using a RAS-*n*SF-IP/EA scheme) are also examined, with particular emphasis on hole and particle excitations.

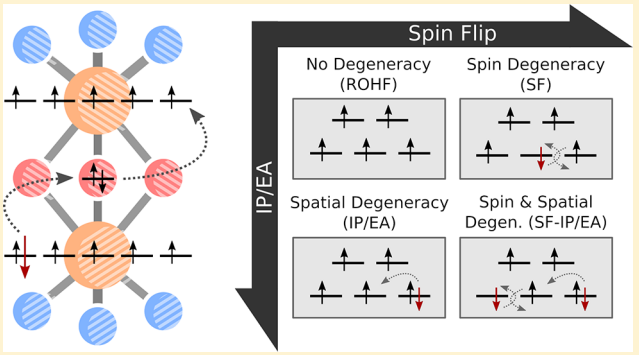

I. INTRODUCTION

Single molecule magnets (SMMs) are molecules which maintain magnetic polarization after the removal of any external magnetic fields. Through a combination of high-spin electronic states, spin−orbit coupling, and crystal field splitting, SMMs exhibit a barrier to magnetic relaxation. This quickly generated initial interest in their potential as high-density data storage devices.[1,2] However, with the growing pursuit of quantum information devices, SMMs have a renewed importance as potential molecular realizations of qubits,[3,4] which has intensified the search for novel SMMs.

Although a high-spin ground state is not a sufficient criterion for creating a SMM, it is indeed an important prerequisite that any SMM should have a stable high-spin or intermediate-spin ground state. Consequently, much work has focused on finding high-spin or intermediate-spin ground state complexes by combining multiple metals coupled by ferromagnetic or ferrimagnetic interactions.[5−7] The famous Mn_{12} SMM is an example where intramolecular exchange stabilizes the intermediate-spin $S = 10$ ground state, which then couples to orbital angular momenta to create a large zero field splitting (ZFS).[8] Unfortunately, the search for strong ferromagnetic exchange couplings is difficult, as "superexchange" is often found to dominate, creating antiferromagnetic coupling (and thus low-spin ground states) in many common coordination patterns. Superexchange, as shown in Figure 1, is a process which couples two magnetic centers (i.e., metal sites) into low-spin states via second order transitions to "ionic" or "charge-resonance" configurations.

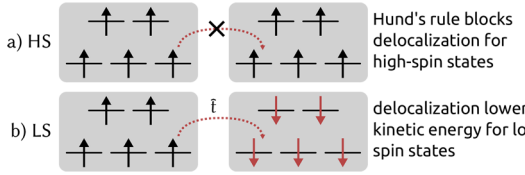

Figure 1. Superexchange: (a) Superexchange is blocked for high spin states as Hund's rule does not allow electron delocalization. (b) Because the two metal centers have different electron spins, delocalization can occur, decreasing the kinetic energy and stabilizing the low-spin state. Note that this can also occur indirectly through a bridging ligand.

One interesting alternative strategy for finding high-spin ground states is to search instead for mixed-valent transition metal systems containing strong "double exchange" interactions. Redox generated mixed-valency has been shown to not only be capable of creating high-spin ground states from low-spin states,[9−11] but also to be responsible for actual SMM behavior in some compounds.[12] Double exchange, originally described by Zener in 1951 to explain magnetic behavior in MnO perovskites,[13] is a mechanism in which the delocalization of an itinerant electron between two high-spin redox centers gives rise to a ferromagnetic exchange interaction. The mechanism is illustrated in Figure 2. The itinerant electron may only move between the orbitals on the redox centers if

Received: December 19, 2018
Published: February 25, 2019

DOI: 10.1021/acs.jctc.8b01268
J. Chem. Theory Comput. 2019, 15, 2278−2290

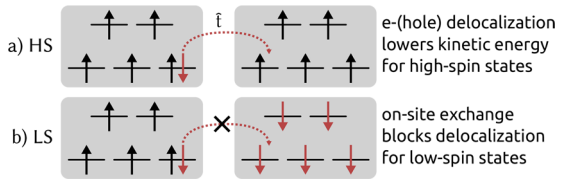

Figure 2. Double exchange: (a) Double exchange due to degenerate electron (or hole) delocalization in a mixed valent compound, stabilizing the high-spin state. (b) Electron delocalization blocked in the low-spin state. Note that while an alpha electron could potentially transfer from left to right, the remaining atom would be left in a high-energy non-Hund state because of strong on-site exchange.

they are ferromagnetically coupled, as illustrated. (Unpaired electrons may also move back and forth between antiferromagnetically coupled orbitals, but because of on-site exchange, these configurations are unfavorable.) The movement of the electron causes an energy splitting that is greater for states with higher spin, and in cases where the splitting is large enough, this causes ferromagnetically coupled states to be favored.

Systems exhibiting this behavior are particularly intriguing in the context of searching for SMMs; the magnetic properties can be altered by simply reducing or oxidizing the molecule.

A few years after Zener's initial paper, Anderson and Hasegawa refined the model to include contributions from non-Hund states which are low-spin atomic configurations.[14] In the early 1980s, there also arose a separate variation on Zener's original model[15] which included an additional parameter, J, accounting for the magnetic coupling between the centers because of the delocalization of the nonitinerant electrons.[16,17] This model Hamiltonian for a symmetric two-center case can be written:

$$\hat{\mathcal{H}}_{\mathrm{ZGP}} = [J^{A}\vec{S}_{A}\cdot{}^{A}\vec{S}_{B} + E]\hat{O}_{A} + [J^{B}\vec{S}_{A}\cdot{}^{B}\vec{S}_{B} + E]\hat{O}_{B} + B\hat{V}_{AB}\hat{T}_{AB} \quad (1)$$

Here, the first two terms are Heisenberg-like (accounting for the coupling J) and the last term accounts for the electron hopping between the centers (analogous to Zener's t). A more detailed description of the ZGP Hamiltonian and its terms can be found on page 4708 of the original ZGP paper.[15] Analytically solving this Hamiltonian yields the following spectrum:[16]

$$E_{\mathrm{ZGP}}(S) = \pm t\frac{S+1/2}{S_{\max}+1/2} - \frac{J}{2}[S(S+1) - S_{\max}(S_{\max}+1)] \quad (2)$$

This was termed the Zener−Girerd−Papaefthymiou (ZGP) model and was so successful that it was often simply referred to in the literature as "the double exchange model". Note that the spectrum given in eq 2 (from Malrieu's work) differs in form from the results given in the Papaefthymiou paper; this is due to the papers' differing definitions of the model Hamiltonian (for example, the sign of J changes, and Malrieu uses a t term analogous to B). To keep our notation consistent across different model Hamiltonians, we will adhere to Malrieu's definitions[16] for the remainder of the text.

Despite the preeminence of ZGP, several studies in the early 2000s highlighted the necessity of including the non-Hund terms,[16,18−21] and a new model combining AH and ZGP (AH-ZGP) was proposed. The analytical solution for a symmetric two-center system is

$$E_{\mathrm{AH\text{-}ZGP}}(S = S_{\max}) = \pm t \quad (3)$$

$$E_{\mathrm{AH\text{-}ZGP}}(S \neq S_{\max}) = \frac{\delta - \sqrt{\delta^2 + 4t\left(t \pm \frac{S+1/2}{S_{\max}+1/2}\delta\right)}}{2} - \frac{J'}{2}[S(S+1) - S_{\max}(S_{\max}+1)] \quad (4)$$

Useful explanations of double exchange and the aforementioned models can also be found in Malrieu's review of SMMs[16] and de Graaf and Broer's book on magnetic interactions.[17] In each of these models, the orbitals are all assumed to have equivalent parameters. In many cases, such as in some iron−sulfur clusters, this is not a valid assumption, and a multiorbital Anderson model must be used. This approach was used in 2014 by Sharma et al, and unlike its predecessors, it does not have an analytical solution.[22]

Computational chemistry is uniquely positioned to aid in the search for, and ultimately the design of, new double-exchange systems. This is due to the microscopic detail afforded by electronic structure calculations, and the ability to perform in silico experiments which are unable to be realized in the lab.

Unfortunately, double exchange systems are inherently difficult to study using ab initio methods. The reason is that, with the electron delocalized between two radical centers, double exchange systems exhibit both **spin** and **spatial** degeneracies (Figure 3), a characteristic which makes single-

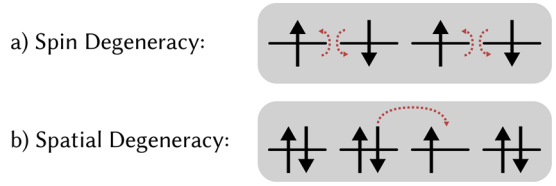

Figure 3. Illustration of spin and spatial degeneracies. (a) Spin degeneracies arise from the inherent degeneracy of α and β spins and are nicely treated by spin-flip methods. (b) Spatial degeneracies arise in mixed-valence situations resulting in electron or hole delocalization and are nicely treated by IP or EA methods.

determinant methods incapable of providing a qualitatively correct description. Density functional theory (DFT) can be used to some success, but problems with symmetry breaking, functional dependence, and the use of ambiguously defined projection formulas complicate the approach.[23−27] Multireference methods such as DDCI[16,28,29] or CASPT2[30,31] perform well but are restrictively expensive for large systems. Krylov's spin-flip (SF) methods provide a single reference alternative for studying systems with spin degeneracy.[32−37] Unlike other CI approaches, SF-CI is also size-extensive, making it ideal for larger multiconfigurational systems.[38,39] We have recently used spin-flip methods to extract parameters from similar systems which are well-modeled by the Heisenberg Hamiltonian.[40−43] However, spin-flip alone is insufficient to describe systems which are also spatially degenerate. Alternatively, for spatially degenerate systems, such as mixed valence compounds or partially occupied degenerate states, methods which change the number of electrons such as ionization potential (IP) or electron affinity (EA) methods can be used with success.[44−52] Both spin-flip and IP/EA methods have also been useful in studies of charge transfer mechanisms.[53] In this Article, we introduce a merger

DOI: 10.1021/acs.jctc.8b01268
J. Chem. Theory Comput. 2019, 15, 2278−2290

of the spin-flip and IP/EA methods to yield an approach (SF-IP or SF-EA), *which can simultaneously treat spin and spatial degeneracies and demonstrate that these are effective methods for studying double exchange complexes.*

II. METHODS: SF-EA/SF-IP

Spin degeneracy is common in diradicals, bond dissociations, and transition metal complexes. To better understand spin degeneracy, let us use the dissociation of neutral diatomic nitrogen as an example. At its natural bonding radius, N_2 has the electron configuration $\sigma^2\pi^4$. Upon dissociation, these bonding orbitals become degenerate with antibonding orbitals σ^* and π^*. The ground state singlet can no longer be represented well by just one electron configuration, and single-reference methods will result in unphysical behavior at the dissociation limit. This spin degeneracy is easily resolved by using Krylov's spin-flip (SF) approach.[32,38] One acts the spin-flip operator on a single-determinant high-spin reference state which is well-defined and single configurational. In the case of N_2, this reference is the $m_s = 7$ state, and a 3-SF can be performed to yield the ground state.

$$|\Psi\rangle = \sum_{i<j<k,\bar{a}<\bar{b}<\bar{c}} c_{ijk}^{\bar{a}\bar{b}\bar{c}} \hat{a}_{ijk}^{\bar{a}\bar{b}\bar{c}} |\Psi^{\mathrm{ROHF}}\rangle \tag{5}$$

Although this is nominally a triple excitation operator, these excitations can be drastically reduced in number by limiting the spin-flipping excitations to occur only among the singly occupied orbitals, while reintroducing external effects one orbital index at a time following the RAS-SF or SF-XCIS approaches.[54−59] This approach additionally restores the spin symmetry lost by starting from a high-spin reference.

Removal of an electron to produce N_2^+ introduces spatial degeneracy into the system. Of the six degenerate orbitals, at least one must always be unoccupied. Which orbital to leave unoccupied is ambiguous, even for the $m_s = 6$ state that spin-flip would use as a reference, and the system becomes multiconfigurational once again. Spin and spatial degeneracies are compared in Figure 3. IP/EA methods, originally developed for calculation of ionization potentials and electron affinities, handle spatial degeneracies quite well.[47,60] They work based on the same principle as spin-flip: Find the closest good single-determinant reference, and act a non-particle-conserving operator on it to obtain the desired state.

In this work, we combine the spin-flip and IP/EA approaches to study systems which exhibit both spin and spatial degeneracies. RAS-*n*SF-IP/EA can be applied in the following way:

1. Find the closest high-spin state that is well-represented by a single determinant, either oxidizing or reducing the system so that all degenerate orbitals have the same electron occupation. Perform a ROHF calculation using this spin state to get the reference wave function, $|\Psi^{\mathrm{ref}}\rangle$.
2. Perform spin-flips and electron additions or eliminations to obtain a basis for the desired sector of Fock space. This is accomplished via non-particle-conserving and non-spin-conserving operators. For example, a 2SF-IP operator is written

$$|\Psi\rangle = \sum_{ijk\bar{a}\bar{b}} c_{ijk}^{\bar{a}\bar{b}} \hat{a}_{ijk}^{\bar{a}\bar{b}} |\Psi^{\mathrm{ref}}\rangle \tag{6}$$

An illustration of the SF-EA approach is shown in Figure 4.

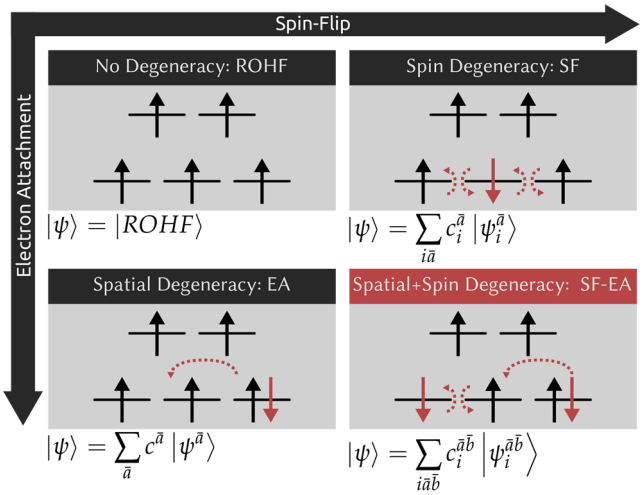

Figure 4. Illustration of the combination of spin-flipping and number changing operators.

Just as with spin-flip models, this formally contains (or is even equivalent to) a CAS calculation (with a different number of electrons) in which the active space is comprised of the singly occupied ROHF orbitals. When the reference is chosen appropriately, the CAS-*n*SF-IP/EA approach is size intensive, as are the RAS(h), RAS(p), RAS(h,p), and RAS(S) schemes described later; however, anything beyond RAS(S)-*n*SF-IP/EA may not be. To explore the features of the RAS-*n*SF-IP/EA approach, we have modified the Psi4[61,62] interface to the DETCI module to produce all the results in this Article. This particular implementation is nonideal from an efficiency perspective, but it is quite general so that different combinations of SF, IP, and EA operators can be explored. Work is currently underway to implement a series of codes optimized for specific combinations of excitation operators for efficient application to larger systems with bigger basis sets.

In the next section, we demonstrate the strength of this approach by applying the RAS-*n*SF-IP/EA strategy to a variety of double-exchange systems, extracting ZGP and AH-ZGP double exchange model Hamiltonian parameters using a method similar to the one used previously for Heisenberg systems.[43] As with the Heisenberg case, the parameters can be extracted from the high and low energy levels of the $S = S_{\mathrm{max}}$ and $S = S_{\mathrm{max}} - 1$ calculations, using only IP/EA and 1SF-IP/EA. (See the Supporting Information for a more thorough explanation of the extraction process.) Thus, *if the model Hamiltonian describes the system well, then the spectrum can be accurately approximated using only inexpensive "partially spin-flipped" states.*

The effects of including additional determinants are also studied. The addition of excitations outside of the traditional CAS-*n*SF-IP/EA active space allows for orbital relaxation. Because the RAS-*n*SF-IP/EA operator is not particle conserving, these relaxations are expected to be highly important for the description of the system. The effects of including the hole (RAS1 → RAS2), particle (RAS2 → RAS3), and hole−particle (RAS1 → RAS3) sets of excitations are studied. (These excitation types are illustrated in Figure 5.) In addition to the full set of singles (h,p,hp), the (h,p) excitation scheme proposed by Casanova and Head-Gordon[54,58] is also implemented. The (h,p) scheme includes only hole (h) and particle (p) excitations, and it is particularly promising because

DOI: 10.1021/acs.jctc.8b01268
J. Chem. Theory Comput. 2019, 15, 2278−2290

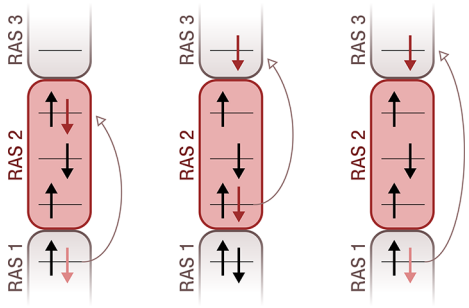

Figure 5. From right to left: The hole (h), particle (p), and hole–particle (hp) types of excitations.

the number of determinants scales linearly with basis set size, assuming that the size of the active space does not change with system size. The overall scaling is thus N^3 if density fitting is used. This makes it ideal for application of RAS-*n*SF-IP/EA to larger systems. To differentiate between schemes, we adopt the notation RAS-*n*SF-IP/EA for the general family of approaches, and CAS-*n*SF-IP/EA for the classic RAS-*n*SF-IP/EA with no additional excitations. Inclusion of hole and particle excitations is denoted by RAS(h)-*n*SF-IP/EA and RAS(p)-*n*SF-IP/EA, while the full set of singles is denoted as RAS(h,p,hp)-*n*SF-IP/EA, or RAS(S)-*n*SF-IP/EA for brevity.

III. RESULTS/DISCUSSION

In this section, we apply the RAS-*n*SF-IP/EA approaches to a variety of systems to illustrate how one can model double exchange compounds. Because equi-valent reference states have an extra electron compared to the target states, SF-IP is

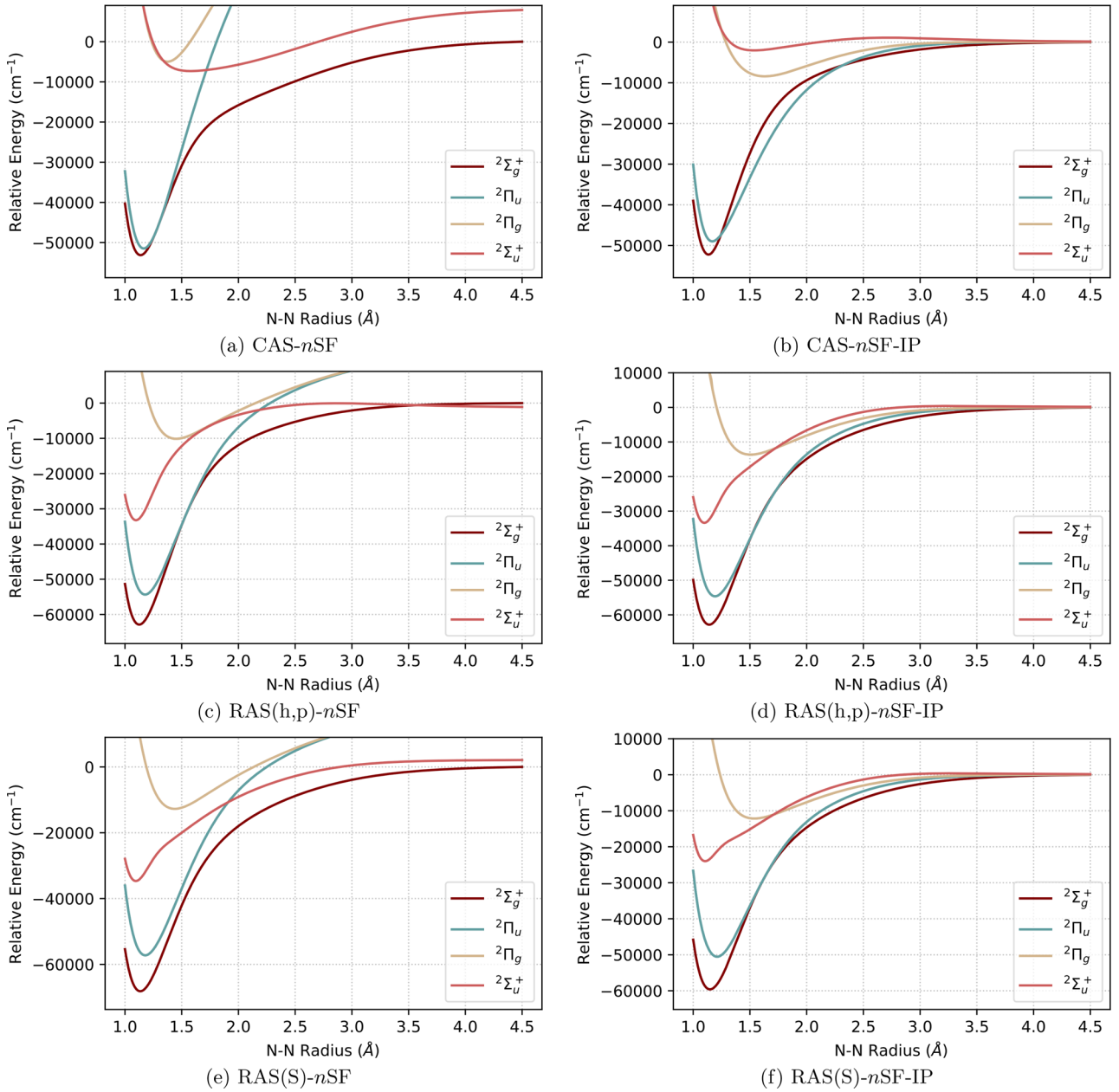

Figure 6. N_2^+ dissociation: (a, c, e) Conventional RAS-*n*SF using cation ROHF $m_s = 6$ as the reference and accessing the $m_s = 2$ states via two spin-flips. (b, d, f) New RAS-*n*SF-IP using neutral ROHF $m_s = 7$ as the reference, and accessing the $m_s = 2$ states via two spin-flips and 1IP excitations.

DOI: 10.1021/acs.jctc.8b01268
J. Chem. Theory Comput. 2019, 15, 2278–2290

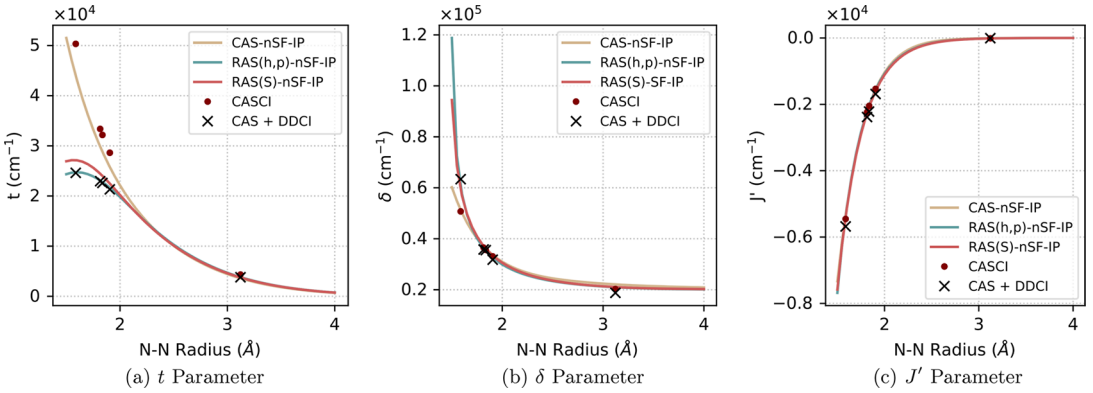

Figure 7. Extracted AH-ZGP parameters t, δ, and J' for N_2^+ with respect to bond length. CAS-CI and CAS + DDCI values obtained from Taratiel et al.[20] (Note that Taratiel's original model Hamiltonian has a sign change in their definition of J'.) The energy scaling for each graph is denoted at the top of the axis.

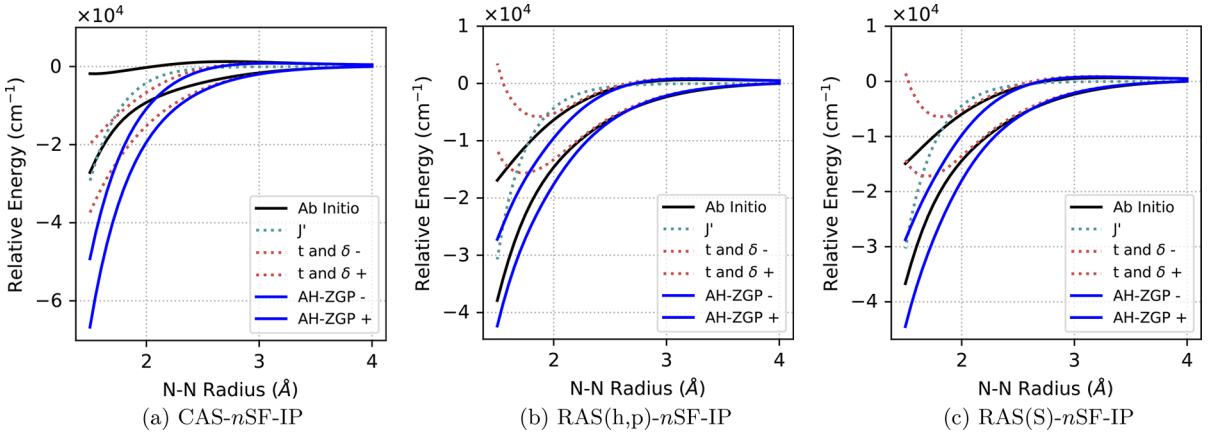

Figure 8. Spectra for $^2\Sigma$ states of N_2^+ cation. Ab initio spectra are labeled as $^2\Sigma$. Plots also include reconstructed spectra using the AH-ZGP model, as well as contributions from the J' term and the $\frac{\delta - \sqrt{\delta^2 + 4t(t \pm \delta/3)}}{2}$ term. Parameters were extracted from the $\Delta_{^6\Sigma_g^+, ^6\Sigma_u^+}$, $\Delta_{^4\Sigma_u^+, ^4\Sigma_g^+}$, and $\Delta_{^4\Sigma_u^+, ^6\Sigma_g^+}$ energy gaps in the RAS-IP and RAS-1SF-IP spectra. Note that the system's deviation from model behavior increases as the nitrogen atoms approach one another. Energy scalings are denoted at the top of each axis.

used to study the N_2^+ cation and $[Re_2OCl_{10}]^{3-}$. In contrast, the nonmixed-valence states for the $[Fe_2(OH)_3(NH_3)_6]^{2+}$ and $[(PY_5Me_2)_2V_2(m\text{-}5,6\text{-dimethylbenzimidazolate})]^{4+}$ compounds have one less electron, and so the SF-EA approach has been applied. The spectra produced allow for simple extraction of model Hamiltonian parameters, which can be compared to both BS-DFT and experimentally determined values. The model Hamiltonian parameters can be determined with only one spin-flip, and in each case the low-spin spectra predicted by the model are checked against the ab initio results for consistency. We also compare our parameters to those previously reported in the literature.

III.A. N_2^+ Cation. As detailed in the introductory section, the diatomic nitrogen cation exhibits both spin and spatial degeneracy at its dissociation limit. When nSF is used to model the doublet states for this system, qualitatively incorrect behavior is predicted at the dissociation limit, where the excited states show divergent rather than the expected convergent behavior (Figure 6a). Conversely, using CAS-nSF-IP with an $m_s = 7$ reference yields excited state energies which become degenerate as $r_{N-N} \to \infty$, as expected. The CAS-nSF-IP results are shown in Figure 6b. All calculations in this section were run with the cc-pVDZ basis set.[63]

III.A.1. Effects of Additional Excitations. Although CAS-2SF-IP shows significant improvement over the CAS-2SF results, there is still qualitative deviation from the experimental spectra.[64] The discrepancy is particularly obvious for the $^2\Sigma_u^+$ curve, which ought to have a much more stable energy minimum and should be significantly lower in energy than the $^2\Pi_g$ state near the bonding radius. Results for RAS(h,p)-2SF-IP and RAS(S)-2SF-IP are shown in Figure 6d and 6f. It is clear that orbital relaxation yields significant qualitative improvement, particularly for the $^2\Sigma_u^+$ curve.

III.A.2. Parameter Extraction. Parameters for the AH-ZGP double exchange Hamiltonian can be extracted from the sextet and quartet Σ^+ states. Here the accuracy of the model can be checked by comparison to results from other ab initio methods. In Figure 7, the extracted parameters are plotted with respect to bond distance and compared against previously reported CAS-CI and CAS + DDCI results.[20] (Note that Taratiel's results use the ANO basis set[65] (10s6p3d contracted in a 7s6p3d) in Molcas, while our results were calculated with the cc-pVDZ basis set.) The CAS-nSF-IP agrees best with CAS-CI, while RAS(h,p)-nSF-IP agrees best with CAS + DDCI. These results clearly illustrate the importance of the (h,p) excitations as the nitrogen atoms approach one another, which is especially pronounced for t. At the dissociation limit,

DOI: 10.1021/acs.jctc.8b01268
J. Chem. Theory Comput. 2019, 15, 2278−2290

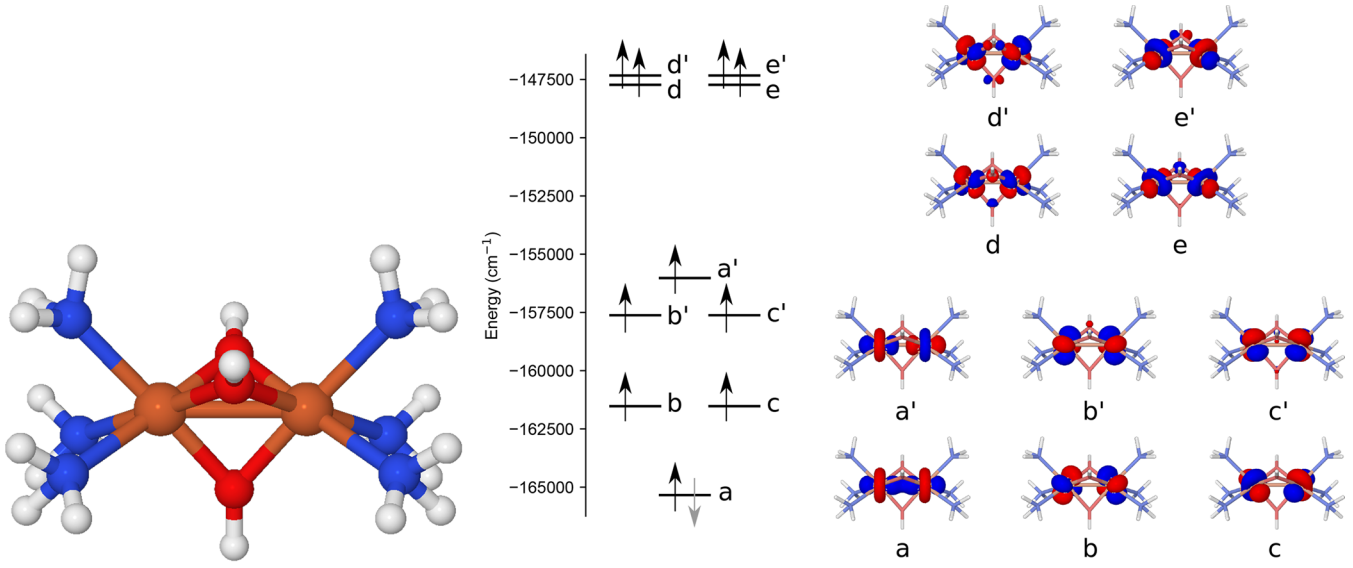

(a) Structure of $[Fe_2(OH)_3(NH_3)_6]^{2+}$. (b) Molecular orbitals of $[Fe_2(OH)_3(NH_3)_6]^{2+}$

Figure 9. Molecular structure and molecular orbital energies of $[Fe_2(OH)_3(NH_3)_6]^{2+}$. The gray electron represents the reduction associated with the EA operator.

Table I. Extracted Double Exchange Model Hamiltonian Parameters for $[Fe_2(OH)_3(NH_3)_6]^{2+}$ (cm^{-1}) and Average Percent Error in Predicting Energy Gaps for the $S = 5/2^-$ and $S = 5/2^+$ States[a]

		ZGP				AH-ZGP				
	$\Delta_{7/2-9/2}$	J	t	% $Err_{5/2-}$	% $Err_{5/2+}$	J'	t	δ	% $Err_{5/2-}$	% $Err_{5/2+}$
CAS-*n*SF-EA	973	−57	6141	0.16	1.81	1.56	6141	41614	0.01	0.02
RAS(h)-*n*SF-EA	874	−63	5788	0.16	1.76	−8.66	5788	39828	0.01	0.01
RAS(p)-*n*SF-EA	1121	−81	7431	0.20	2.32	−2.87	7431	44196	0.01	0.03
RAS(h,p)-*n*SF-EA	1055	−84	7161	0.20	2.31	−8.65	7161	42716	0.01	0.02
CASSCF	913	−103	6895	0.41	2.39					
CASPT2	1066	−58	6625	2.93	21.08					
DFT	752	−137	6830							
exp.	>720	$\lvert J\rvert$ < 140	6750							

[a]Percent errors are calculated relative to the full spectrum width; see eq 7 for details. Experimental,[9] DFT,[24] and CAS[66] results are reported for comparison.

the J' and t terms approach zero, as expected, while the δ term accounting for non-Hund states approaches 20 000 cm^{-1} (2.4 eV). This is a sensible value because at infinite distance, the value of δ should be similar to the doublet-quartet gap for a single nitrogen atom, which at the 1SF-CAS level is 23 462 cm^{-1}. As the nitrogen atoms approach one another, the hopping term t increases; note that it reaches a maximum for the (h,p) and S excitation schemes (agreeing with CAS + DDCI) while the CAS-*n*SF-IP results simply continue to increase (agreeing with CAS-CI). This indicates that the single excitations are both effective and necessary for accurately capturing double exchange behavior.

The AH-ZGP results can also be validated by testing their self-consistency. Because the system is overdefined, the doublet energy spectrum can be recalculated and analyzed for deviation from the ab initio spectrum. The predicted energy contributions from J' and the combined t and δ term are plotted in Figure 8. The antiferromagnetic coupling J only comes into effect near the bonding radius; the combined t and δ term contributes the most in the 1−2 Å range. As the nitrogen atoms move closer to one another, the double exchange Hamiltonian is no longer sufficient to describe the system, causing deviation in the predicted spectra.

III.B. $[Fe_2(OH)_3(NH_3)_6]^{2+}$. The $[Fe_2(OH)_3(tmtacn)_2]^{2+}$ mixed-valent complex has been studied extensively in the literature.[9,10,24,66,67] Its ground state is $S = 9/2$, with iron oxidation states of Fe^{3+} and Fe^{2+}. A simplified version of the system in which the ligands are replaced with NH_3 groups ($[Fe_2(OH)_3(NH_3)_6]^{2+}$, shown in Figure 9a) has previously been studied with many computational methods, including SCF-Xα-SW,[9] BS-DFT,[24] and CASPT2.[66,67] Here, *n*SF-EA is applied to the idealized geometry used for the SCF-Xα-SW calculations in Gamelin's work.[9] The cc-pVDZ basis set was used for all atoms.[63,68] For all calculations involving particle excitations, the highest 74 virtual orbitals were frozen due to limitations on the number of active space orbitals permitted by Psi4's DETCI module. However, as mentioned above, we are currently working on a fixed-excitation rank version of the theory which will provide a much more efficient (but less flexible) code.

The orbitals and orbital energies of the singly occupied orbitals from the single-determinant reference ROHF calculation are shown in Figure 9b. To obtain the desired $S = 9/2$ state from the $S = 5$ reference, an electron addition is performed. The most stable high-spin configuration places this extra electron in the lowest-energy orbital (labeled as orbital a

DOI: 10.1021/acs.jctc.8b01268
J. Chem. Theory Comput. 2019, 15, 2278−2290

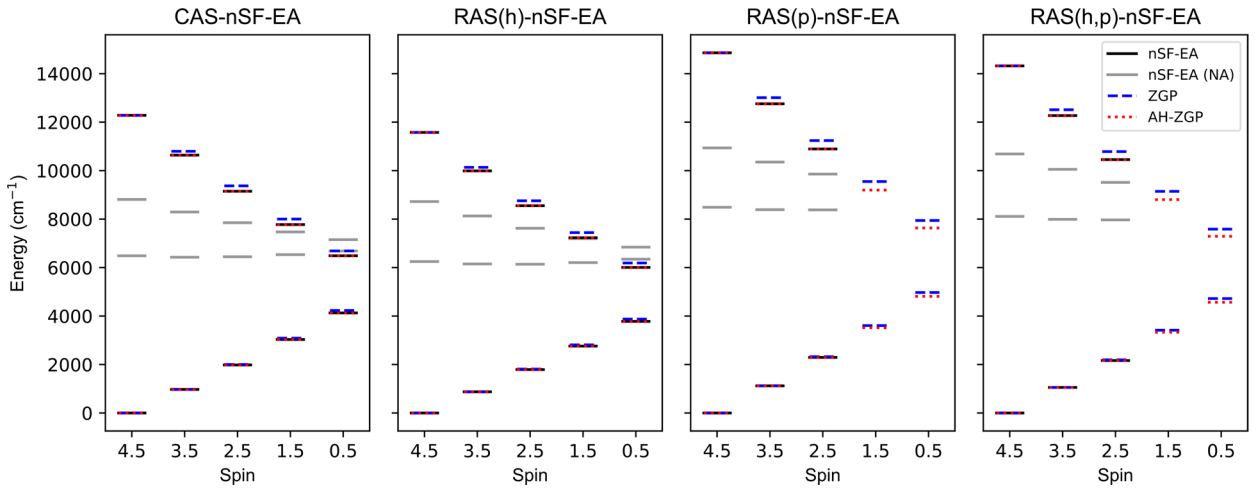

Figure 10. Ab initio and reconstructed energy spectra of $[Fe_2(OH)_3(NH_3)_6]^{2+}$ using the AH-ZGP or ZGP parameters obtained from the specified methods. Non-Aufbau states are denoted by (NA).

in Figure 9b). The delocalization of the electron between orbital a and the corresponding antibonding orbital a′ will produce two states, which should be well-modeled by a double exchange Hamiltonian. There are also two low-lying degenerate orbitals, b and c, which, when doubly occupied, produce two pairs of doubly degenerate non-Aufbau states because of electron delocalization between these orbitals and b′ and c′ respectively. On the basis of the relative energies of the orbitals, these states will likely lie between the double exchange states.

III.B.1. Spectra and Extracted Parameters. Model Hamiltonian parameters for the ZGP and AH-ZGP models were extracted from the EA and 1SF-EA calculations and are reported in Table I. The ZGP parameters J and t were extracted from the $\Delta_{9/2^-,9/2^+}$ and $\Delta_{9/2^-,7/2^-}$ energy gaps. Also reported in the table for the sake of comparison are experimental[9] and DFT[24] results, as well as Carissan's CASSCF and CASPT2 results.[66] Our values show reasonable agreement with these previously reported results. The energy gap between the two lowest-lying spin states can also help provide validation of the *n*SF-EA spectra. Gamelin's experimental results[9] give a lower bound of $\Delta_{7/2-9/2} > 720$ cm^{-1}. Our CAS-1SF-EA and RAS(h,p)-1SF-EA produce values of 973 and 1055 cm^{-1}, respectively. These are in good agreement with the CASSCF value of 913 cm^{-1} and the CASPT2 value of 1066 cm^{-1} from the literature[66] but significantly differ from the DFT value of 752 cm^{-1}.

The AH-ZGP parameters t, J', and δ were also extracted from the $\Delta_{9/2^-,9/2^+}$, $\Delta_{9/2^-,7/2^-}$ and $\Delta_{9/2^-,7/2^+}$ gaps. (We were unable to extract AH-ZGP parameters for Carissan's values.) The ab initio spectra and the spectra predicted by the model Hamiltonians are shown in Figure 10. Note that the $S = 3/2$ and $S = 1/2$ states could not be calculated for the (p) and (h,p) schemes with this preliminary implementation because of the size of the calculation. The ZGP values seem qualitatively reasonable for most cases but show some deviation, particularly for the high-energy states. This is especially clear in Carissan's CASPT2 spectrum, where the values predicted by the ZGP model deviate significantly from the true ab intio values. The errors of the predicted spectra relative to the true ab initio values for the $S = 5/2$ states, reported in Table I, show that AH-ZGP (average error of 0.01% for the RAS-*n*SF-EA methods) predicts the low-spin spectra significantly better than the ZGP model (average error of 1.12%). Errors were calculated as a percent of the full spectrum width using the equation

$$\%\mathrm{Err}_{5/2^\pm} = \frac{|E^{\mathrm{model}}_{5/2^\pm} - E^{\mathrm{SF-EA}}_{5/2^\pm}|}{\Delta E_{9/2^+,9/2^-}} \times 100\% \quad (7)$$

where $5/2^-$ and $5/2^+$ denote the low- and high-energy $S = 5/2$ states, respectively, and $\Delta E_{9/2^+,9/2^-}$ denotes the full spectrum width (which in this case is the energy gap between the $S = 9/2$ states).

The AH-ZGP model seems to successfully replicate the spectra for the RAS-*n*SF-EA case, implying that non-Hund states are important to consider when modeling this system. The average errors including errors for $S = 3/2$ and $S = 1/2$ states of CAS-*n*SF-EA and RAS(h)-*n*SF-EA, reported in the Supporting Information section, are slightly larger, implying that there is more deviation the further the values are extrapolated; however, the values do not deviate much, and AH-ZGP seems to work well even for the lowest-spin states.

For larger systems, it will likely only be possible to include a subset of the single excitations, so we will take this opportunity to explore the effects of including hole and particle excitations. It is clearly evident in Figure 10 that the (p) scheme produces the spectrum closest to that of (h,p). This is quantitatively confirmed by the average percent errors of the ab initio energy gaps for CAS-*n*SF-EA, RAS(h)-*n*SF-EA, and RAS(p)-*n*SF-EA schemes relative to the RAS(h,p)-*n*SF-EA energy gaps, which are 7.32%, 10.45%, and 2.32%, respectively. (Errors were taken as a percent of the full RAS(h,p)-*n*SF-EA spectrum width.)

It is also interesting to note that for the RAS-*n*SF-EA calculations, the inclusion of additional excitations does not reduce the accuracy of the double exchange model's predictions, as is normally expected because of the wave function developing larger weights on configurations outside of the model space. (In fact, this behavior can be seen when comparing the CASSCF and CASPT2 results.) Although somewhat unexpected, this is sensible, as the active space into which the electron is added is negatively charged by the addition of an extra electron; allowing orbital relaxation delocalizes the charge, allowing the extra electron to move without the charge bias, and gives a better description of the system. The improved performance of (p) relative to (h) can

DOI: 10.1021/acs.jctc.8b01268
J. Chem. Theory Comput. 2019, 15, 2278−2290

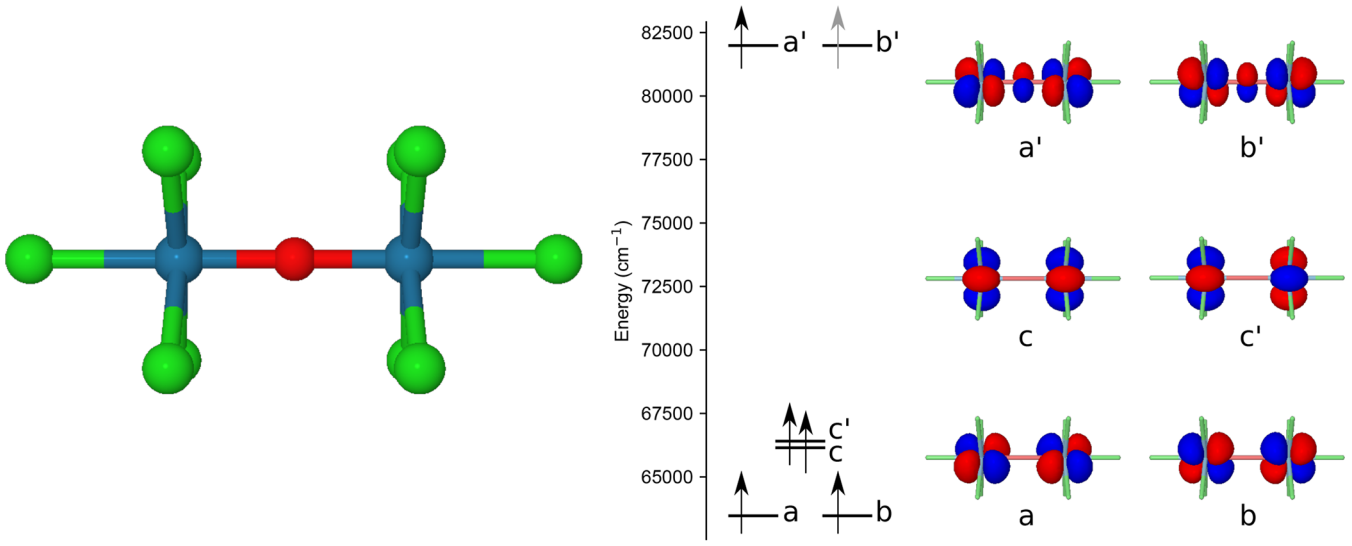

(a) Structure of $[Re_2OCl_{10}]^{3-}$. (b) Molecular orbitals of $[Re_2OCl_{10}]^{3-}$.

Figure 11. Molecular structure and molecular orbital energies of $[Re_2OCl_{10}]^{3-}$.

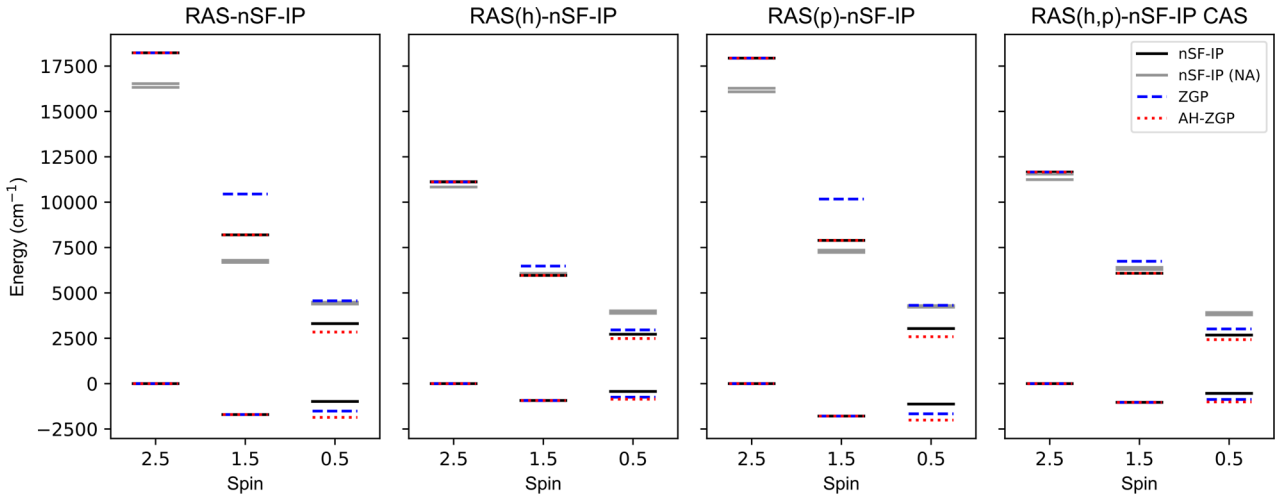

Figure 12. Ab initio and reconstructed energy spectra of $[Re_2OCl_{10}]^{3-}$. Non-Aufbau states are denoted by (NA).

be explained similarly; particle excitations allow the extra negative charge to spread out into the virtual space, while hole excitations would force even more charge into the active space. *Because of this, particle excitations are more important for EA calculations, whereas hole excitations are more important for IP calculations.* As a result, we view the minimally accurate models (or zeroth-order models) to be RAS(p)-nSF-EA and RAS(h)-nSF-IP.

III.C. $[Re_2OCl_{10}]^{3-}$. The $[Re_2OCl_{10}]^{3-}$ complex (Figure 11a) has been studied both experimentally[69] and with CASCI and DDCI methods.[19] There are three possible spin states for this system: $S = 1/2$, $S = 3/2$, and $S = 5/2$. Interestingly, this molecule's ground state is the quartet. Here, RAS-*n*SF-IP calculations have been performed on the geometry taken from the experimental crystal structure.[69] The LANL2DZ basis set[70] has been used for the Re atoms, while the cc-pVDZ basis set[63,71] has been used for all others.

The ROHF reference orbitals and their orderings are shown in Figure 11b. The field splittings are typical of those for a complex with near-octahedral geometry. Note that the lowest two orbitals are the degenerate antibonding d_{xy} and d_{yz} orbitals. The antibonding orbitals are lowest in energy because the mixing of bonding d_{xy} and d_{yz} orbitals on the Re with the p orbital on the bridging O results in an energy raising of the bonding orbitals. The antibonding d_{xy} and d_{yz} orbitals are unaffected because they are unable to mix with the p orbitals of the bridging ligand. This is consistent with orderings reported in previous literature.[19,72]

Unlike the previous example, this complex requires the removal of one electron (IP). The most stable removal will be from one of the two near-degenerate highest-energy orbitals (a′ or b′), so each of the two nearly degenerate ground states will be stabilized by delocalization of the hole between one of these orbitals and the corresponding bonding orbital (a or b), rather than delocalization of an itinerant β electron. Each bonding/antibonding pair is expected to produce two states; since the orbitals themselves are nearly degenerate, the states should be nearly degenerate as well, leading to two sets of doubly degenerate states in the spectrum. The nondegenerate orbitals (c and c′) can also take on the hole to produce two additional non-Aufbau states.

DOI: 10.1021/acs.jctc.8b01268
J. Chem. Theory Comput. 2019, 15, 2278−2290

Table II. Extracted Double Exchange Model Hamiltonian Parameters for $[Re_2OCl_{10}]^{3-}$ (cm^{-1}) and Average Percent Error in Predicting Energy Gaps for the $S = 1/2$ State[a]

	ZGP				AH-ZGP				
	J	t	% $Err_{1/2-}$	% $Err_{1/2+}$	J'	t	δ	% $Err_{1/2-}$	% $Err_{1/2+}$
CAS-*n*SF-IP	−1897	9115	2.66	6.30	−1370	9115	21508	4.40	2.34
RAS(h)-*n*SF-IP	−1113	5557	2.63	1.98	−885	5557	22161	3.54	1.95
RAS(p)-*n*SF-IP	−1911	8968	2.72	6.49	−1386	8968	20820	4.48	2.29
RAS(h,p)-*n*SF-IP	−1190	5830	2.65	2.65	−933	5830	20974	3.69	1.98
CAS(5,6)CI	−1831	9737	16.58	3.88	−1154	9737	16468	3.54	1.61
CAS(5,6)+DDCI2	−2010	7972	5.50	2.11	−1622	7972	24739	6.70	3.43
CAS(9,8)+DDCI2	−2348	8239	8.54	0.37	−2000	8239	31531	9.42	4.20
CAS(5,6)CI[b]	−2637	9737	16.57	3.87	−1007	9737	15523	1.22	0.01
CAS(5,6)+DDCI2[b]	−2250	7972	10.73	3.12	−1293	7972	19433	1.32	0.02
CAS(9,8)+DDCI2[b]	−2513	8239	11.91	3.74	−1533	8239	21296	2.57	0.04

[a]CASCI values from previous work[19] are reported for comparison. ZGP's J was calculated based on the average of quartets. [b]Parameters extracted as in the original paper, rather than using sextet and quartet only.

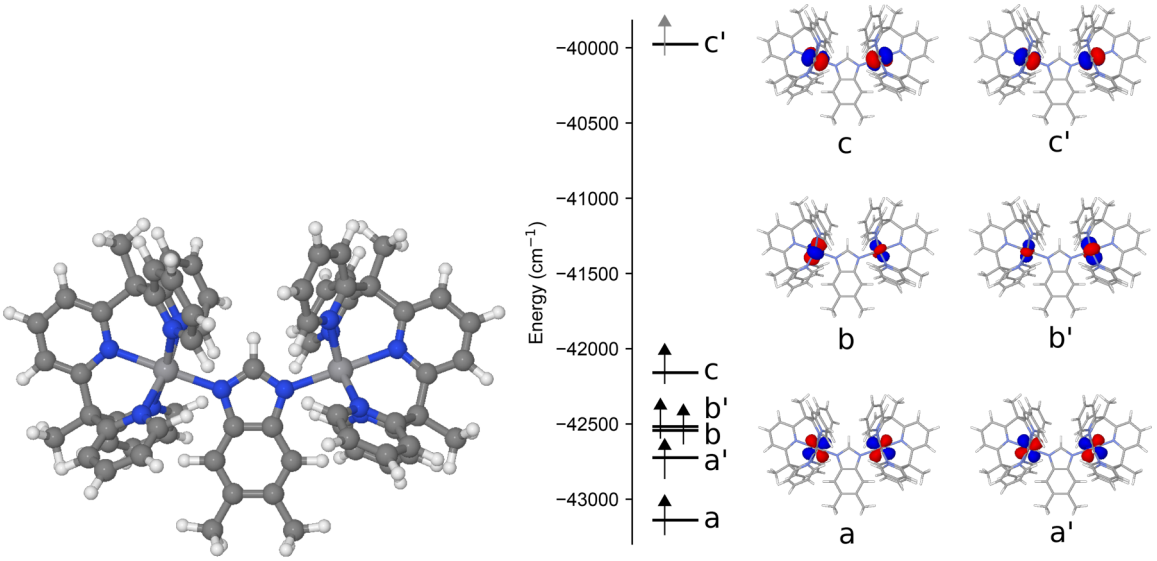

(a) Structure of di-vanadium complex. (b) Molecular orbitals of di-vanadium complex.

Figure 13. Molecular structure and molecular orbital energies of $[(PY_5Me_2)_2V_2(m\text{-}5,6\text{-dimethylbenzimidazolate})]^{4+}$.

III.C.1. Spectra and Extracted Parameters. The ab initio energy spectra are shown in Figure 12. (The RAS(S)-*n*SF-IP/EA spectra were also calculated for the $S = 5/2$ and $S = 3/2$ states and showed similar behavior. The relevant values and parameters can be found in the Excel sheet for this compound in the Supporting Information.) The ground state in all cases is the quartet, which is consistent with the experimental data. Note that all ground states are doubly degenerate. The nondegenerate non-Aufbau states are also reported, as well as the recalculated spectra from the ZGP and AH-ZGP model Hamiltonians, where parameters have been extracted based only on the doubly degenerate $S = 5/2$ and $S = 3/2$ ground and excited states. Parameters for the model Hamiltonian spectra are reported in Table II, as well as the extracted parameters reported by Guihéry for comparison.[19] Note that in Guihéry's original paper, the AH-ZGP parameters are extracted based on the entire spectrum, rather than just the two highest-spin states. Two sets of parameters for Guihéry's results are reported in the table: the values originally reported in the paper, and values that were re-extracted using $\Delta_{5/2-,3/2-}$ (whereas the original paper used the averages of the $S = 5/2$ and $S = 3/2$ states). The CAS-*n*SF-IP and RAS(p)-*n*SF-IP seem to yield the closest values to Guihéry's highest-level results, but in both cases, this is likely due to fortuitous error cancellation, since the RAS(h,p)-*n*SF-IP (our most accurate level of theory) shows greater deviation from the DDCI2 values. (Guihéry's results include 2-hole and 2-particle excitations and therefore include dynamical correlations that our results lack, which may help account for the discrepancy.)

As before, the accuracy of the model Hamiltonians can also be evaluated by analyzing their ability to reconstruct the doublet energy levels. Percent errors are shown in Table II. In this case, the AH-ZGP provides little improvement over ZGP, and in fact actually provides a worse fit in some cases. Using the $S = 1/2$ energy levels for the extraction as done in Guihéry's previous work yields a significantly better fit; however, if the AH-ZGP model Hamiltonian truly describes the system well, it should not matter which energy levels are used for the parameter extraction. The inconsistency indicates that the AH-ZGP is not a sufficient theory, and a different model may be ultimately necessary. It is possible that the multiorbital AH-ZGP model as proposed by Sharma et al.[22] will provide a better prediction. This approach will be

DOI: 10.1021/acs.jctc.8b01268
J. Chem. Theory Comput. 2019, 15, 2278−2290

addressed in our future work, using a Bloch effective Hamiltonian to extract the Hamiltonian parameters.

As before, it is useful to compare the different excitation schemes. Here the RAS(h)-*n*SF-IP scheme seems to give the closest approximation of the RAS(h,p)-*n*SF-IP energy gaps, with an average error of 1.44% relative to the full spectrum width, while the energy gaps of CAS-*n*SF-IP and RAS(p)-*n*SF-IP have an error of 16.44% and 15.43% on average, respectively. (Calculations of individual percent errors can be found in the Supporting Information.) This is expected, as when the electron has been eliminated, relaxing the core orbitals to allow other electrons enter the hole created in the active space is somewhat more important than relaxing the virtual orbitals. This confirms that IP calculations ought to prioritize the inclusion of hole excitations. Also, as before, the addition of excitations does not seem to have a negative effect on the accuracy of the extrapolations for the low-spin states.

III.D. Hole Delocalization in Divanadium Complex. The divanadium complex $[(PY_5Me_2)_2V_2(m\text{-}5,6\text{-dimethylbenzimidazolate})]^{4+}$, shown in Figure 13(a), is one of the more recently discovered systems exhibiting double exchange. It was initially synthesized and studied experimentally by Bechlars et al.[11] and was subsequently studied with a combined DFT/TD-DFT methodology by Ghosh et al.[73] Like the previous complex, this double exchange system can also be thought of in terms of hole delocalization, so the RAS-*n*SF-IP methodology has been applied. Ghosh's DFT-optimized geometry for the high-spin $S = 5/2$ state was used for all calculations in this section, and the 6-31G basis[74,75] was used due to the molecule's size.

The molecular orbitals from the ROHF reference are shown in Figure 13(b). Since this is a hole delocalization and the most favorable removal is from the highest-energy orbital, the two lowest-energy states should have delocalization of the hole across the highest (antibonding) orbital and the corresponding bonding orbital. In this case, due to the spacings of the MOs, the non-Aufbau states are expected to be higher in energy and are therefore unlikely to interact.

III.D.1. Spectra and Extracted Parameters. The ab initio and reconstructed energy levels are shown in Figure 14, and the extracted parameters and average percent errors when reconstructing the doublet state energy levels are reported in Table III. Note that only CAS-*n*SF-IP calculations were fully completed due to difficulties with convergence in the CI steps. The RAS(h)-*n*SF-IP was completed for only the $S = 5/2$ state, so the t value could be extracted. For RAS(h)-*n*SF-IP, the lowest 89 molecular orbitals were frozen to reduce the calculation size. We plan to revisit this complex with the new excitation-rank code, which will evaluate the Hamiltonian via uniquely defined tensor contractions rather than using a string-based approach.

Unlike in the previous case, the non-Aufbau states do not become close in energy with the lowest-lying ones. The ZGP model works much better for this system than the previous ones (error of <0.2%), likely because of this lack of mixing. Both models are able to predict the low-spin energy levels with a high level of accuracy, and although the AH-ZGP model does perform slightly better, ZGP is accurate enough that AH-ZGP is likely unnecessary for good prediction of the spectra for this system.

Comparing our ZGP parameters to experimental data is difficult because different experiments have shown somewhat inconsistent values, partially due to vibronic coupling present in the molecule.[11] Accordingly, Bechlars et al. have extracted the parameters in two ways: Once from temperature-dependent magnetic susceptibility measurements, and once from the optical data including vibronic effects. For the optical extraction, it is assumed that the exchange term J is unchanged by the removal of an electron (although the validity of this assumption is challenged by a subsequent DFT/TD-DFT study). Our J agrees quite well with the one extracted from the magnetic susceptibility measurement, while the t term agrees best with the one from the optical rotation extraction. Both agree better with the experimental values than they do with DFT.

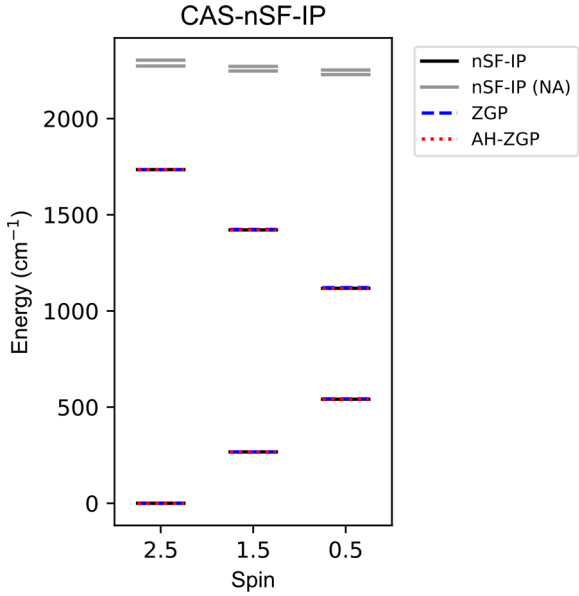

Figure 14. Ab initio and reconstructed energy spectra of $[(PY_5Me_2)_2V_2(m\text{-}5,6\text{-dimethylbenzimidazolate})]^{4+}$. Non-Aufbau states are denoted by (NA).

IV. CONCLUSIONS

In this work, we have proposed the use of redox spin-flip operators, RAS-*n*SF-IP and RAS-*n*SF-EA, to accurately study molecules which exhibit simultaneous spin and spatial degeneracies. We have shown the efficacy of the model by applying it to various double exchange systems. Parameters for the ZGP and AH-ZGP double exchange model Hamiltonians have been extracted from the IP/EA and *n*SF-IP/EA spectra, and the effectiveness of this extraction method has been evaluated both by its ability to accurately predict the energy gaps for the lower-spin states and by comparison to previously published data.

Additionally, the importance of including hole and particle excitations is studied. The hole excitations are shown to be most important for the calculations involving an electron elimination, while particle excitations are most important for electron additions. Allowing orbital relaxation through these excitations is incredibly important for RAS-*n*SF-IP/EA methods because of the non-particle-conserving nature of the operator. Because the number of parameters required for the hole and particle excitation schemes have linear scaling with respect to basis set size, they allow reasonable accuracy for RAS-*n*SF-IP/EA methods when modeling molecules which are too large for the full set of single excitations.

DOI: 10.1021/acs.jctc.8b01268
J. Chem. Theory Comput. 2019, 15, 2278−2290

Table III. Extracted Double Exchange Model Hamiltonian Parameters for $[(PY_5Me_2)_2V_2(m\text{-}5,6\text{-dimethylbenzimidazolate})]^{4+}$ (cm^{1-}) and Percent Error in Predicting Energy Gaps for the Low-Spin States[a]

	ZGP				AH-ZGP				
	J	t	% $Error_{1/2-}$	% $Error_{1/2+}$	J'	t	δ	% $Error_{1/2-}$	% $Error_{1/2+}$
CAS-*n*SF-IP	−8.9	868	0.11	0.19	−6.24	868	47834	0.08	0.02
RAS(h)-*n*SF-IP		864							
DFT	−30.8	1998							
exp. (Magnetic Susceptibility)	−8.8	366							
exp. (optical)	−12	660							

[a]Experimental[11] and DFT[73] results from previous literature are reported for comparison.

We believe that the RAS-*n*SF-IP/EA approach shows great promise for accurate modeling of relatively large complexes with simultaneous spin and spatial degeneracy, such as double exchange-stabilized high-spin complexes. In the future, we plan to extend this method to larger systems with optimized implementations and to apply Bloch effective Hamiltonians to the modeling of more complicated Hamiltonians such as the multiorbital Anderson model. We will also apply the model to double exchange systems with more than two metal sites, as well as other SMMs. Additionally, we plan to study the effects of vibrational frequencies (for example, bond stretching between the redox centers and ligands) on the couplings and exchange mechanisms present in these systems.

■ ASSOCIATED CONTENT

Supporting Information

The Supporting Information is available free of charge on the ACS Publications website at DOI: 10.1021/acs.jctc.8b01268.

Additional details regarding extraction of the model Hamiltonian parameters(PDF)

XYZ coordinate files for $[Fe_2(OH)_3(NH_3)_6]^{2+}$ (XYZ)

XYZ coordinate files for $[Re_2OCl_{10}]^{3-}$ (XYZ)

XYZ coordinate files for divanadium (XYZ)

Raw data and parameter extractions for N_2 and its cation (XLSX)

Raw data and parameter extractions for $[Fe_2(OH)_3(NH_3)_6]^{2+}$ (XLSX)

Raw data and parameter extractions for $[Re_2OCl_{10}]^{3-}$ (XLSX)

Raw data and parameter extractions for divanadium (XLSX)

■ AUTHOR INFORMATION

Corresponding Author

*E-mail: nmayhall@vt.edu.

ORCID

Nicholas J. Mayhall: 0000-0002-1312-9781

Notes

The authors declare no competing financial interest.

■ ACKNOWLEDGMENTS

The authors would like to acknowledge the Virginia Tech chemistry department and the Psi4 community for useful discussion. We would also like to acknowledge funding from the Department of Energy grant DE-SC0018326.

■ REFERENCES

(1) Krusin-Elbaum, L.; Shibauchi, T.; Argyle, B.; Gignac, L.; Weller, D. Stable ultrahigh-density magneto-optical recordings using introduced linear defects. *Nature* **2001**, *410*, 444−446.

(2) Ruiz-Molina, D.; Mas-Torrent, M.; Gómez, J.; Balana, A. I.; Domingo, N.; Tejada, J.; Martínez, M. T.; Rovira, C.; Veciana, J. Isolated Single-Molecule Magnets on the Surface of a Polymeric Thin Film. *Adv. Mater.* **2003**, *15*, 42−45.

(3) Thiele, S.; Balestro, F.; Ballou, R.; Klyatskaya, S.; Ruben, M.; Wernsdorfer, W. Electrically driven nuclear spin resonance in single-molecule magnets. *Science* **2014**, *344*, 1135−1138.

(4) Vincent, R.; Klyatskaya, S.; Ruben, M.; Wernsdorfer, W.; Balestro, F. Electronic read-out of a single nuclear spin using a molecular spin transistor. *Nature* **2012**, *488*, 357−360.

(5) Moragues-Cánovas, M.; Helliwell, M.; Ricard, L.; Rivière, É.; Wernsdorfer, W.; Brechin, E.; Mallah, T. An Ni_4 Single-Molecule Magnet: Synthesis, Structure and Low-Temperature Magnetic Behavior. *Eur. J. Inorg. Chem.* **2004**, *2004*, 2219−2222.

(6) Shiga, T.; Miyasaka, H.; Yamashita, M.; Morimoto, M.; Irie, M. Copper(II)-terbium(III) Single-Molecule Magnets linked by photochromic ligands. *Dalton Trans* **2011**, *40*, 2275−2282.

(7) Kühne, I. A.; Kostakis, G. E.; Anson, C. E.; Powell, A. K. An Undecanuclear Ferrimagnetic Cu_9Dy_2 Single Molecule Magnet Achieved through Ligand Fine-Tuning. *Inorg. Chem.* **2016**, *55*, 4072−4074.

(8) Sessoli, R.; Tsai, H.-L.; Schake, A. R.; Wang, S.; Vincent, J. B.; Folting, K.; Gatteschi, D.; Christou, G.; Hendrickson, D. N. High-Spin Molecules: $[Mn_{12}O_{12}(O_2CR)_{16}(H_2O)_4]$. *J. Am. Chem. Soc.* **1993**, *115*, 1804−1816.

(9) Gamelin, D. R.; Bominaar, E. L.; Kirk, M. L.; Wieghardt, K.; Solomon, E. I. Excited-State Contributions to Ground-State Properties of Mixed-Valence Dimers: Spectral and Electronic-Structural Studies of $[Fe_2(OH)_3(tmtacn)_2]^{2+}$ Related to the $[Fe_2S_2]^+$ Active Sites of Plant-Type Ferredoxins. *J. Am. Chem. Soc.* **1996**, *118*, 8085−8097.

(10) Drüeke, S.; Chaudhuri, P.; Pohl, K.; Wieghardt, K.; Ding, X.-Q.; Bill, E.; Sawaryn, A.; Trautwein, A. X.; Winkler, H.; Gurman, S. J. The Novel Mixed-valence, Exchange-coupled, Class III Dimer $[L_2Fe_2(\mu\text{-}OH)_3]^{2+}$ (L = N,N′,N″-Trirnethyl-1,4,7-triazacyclononane). *J. Chem. Soc., Chem. Commun.* **1989**, 59−62.

(11) Bechlars, B.; D'Alessandro, D. M.; Jenkins, D. M.; Iavarone, A. T.; Glover, S. D.; Kubiak, C. P.; Long, J. R. High-spin ground states via electron delocalization in mixed-valence imidazolate-bridged divanadium complexes. *Nat. Chem.* **2010**, *2*, 362−368.

(12) Tong, J.; Demeshko, S.; John, M.; Dechert, S.; Meyer, F. Redox-Induced Single-Molecule Magnetism in Mixed-Valent [2 × 2] Co $_4$Grid Complexes. *Inorg. Chem.* **2016**, *55*, 4362−4372.

(13) Zener, C. Interaction between the *d*-Shells in the Transition Metals. II. Ferromagnetic Compounds of Manganese with Perovskite Structure. *Phys. Rev.* **1951**, *82*, 403−405.

(14) Anderson, P. W.; Hasegawa, H. Considerations on Double Exchange. *Phys. Rev.* **1955**, *100*, 675−681.

(15) Papaefthymiou, V.; Girerd, J. J.; Moura, I.; Moura, J. J. G.; Münck, E. Mössbauer Study of D. *gigas* Ferredoxin II and Spin-

DOI: 10.1021/acs.jctc.8b01268
J. Chem. Theory Comput. 2019, 15, 2278−2290

Coupling Model for the Fe_3S_4 Cluster with Valence Delocalization. *J. Am. Chem. Soc.* **1987**, *109*, 4703−4710.
(16) Malrieu, J. P.; Caballol, R.; Calzado, C. J.; de Graaf, C.; Guihéry, N. Magnetic Interactions in Molecules and Highly Correlated Materials: Physical Content, Analytical Derivation, and Rigorous Extraction of Magnetic Hamiltonians. *Chem. Rev.* **2014**, *114*, 429−492.
(17) de Graaf, C.; Broer, R. *Magnetic Interactions in Molecules and Solids*; Springer, 2016.
(18) Guihéry, N.; Malrieu, J. P. The double exchange mechanism revisited: An ab initio study of the $[Ni_2(napy)_4Br_2]^+$ complex. *J. Chem. Phys.* **2003**, *119*, 8956−8965.
(19) Guihéry, N. The double exchange phenomenon revisited: the $[Re_2OCl01]^{3-}$ compound. *Theor. Chem. Acc.* **2006**, *116*, 576−586.
(20) Taratiel, D.; Guihéry, N. A refined model of the double exchange phenomenon: Test on the stretched N_2^+ molecule. *J. Chem. Phys.* **2004**, *121*, 7127−7135.
(21) Bastardis, R.; Guihéry, N.; de Graaf, C. Ab initio study of the Zener polaron spectrum of half-doped manganites: Comparison of several model Hamiltonians. *Phys. Rev. B: Condens. Matter Mater. Phys.* **2006**, *74*, 014432.
(22) Sharma, S.; Sivalingam, K.; Neese, F.; Chan, G. K.-L. Low-energy spectrum of iron-sulfur clusters directly from many-particle quantum mechanics. *Nat. Chem.* **2014**, *6*, 927−933.
(23) Boilleau, C.; Suaud, N.; Bastardis, R.; Guihéry, N.; Malrieu, J. P. Possible use of DFT approaches for the determination of double exchange interactions. *Theor. Chem. Acc.* **2010**, *126*, 231−241.
(24) Barone, V.; Bencini, A.; Ciofini, I.; Daul, C. A.; Totti, F. Density Functional Modeling of Double Exchange Interactions in Transition Metal Complexes. Calculation of the Ground and Excited State Properties of $[Fe_2(OH)_3(tmtacn)_2]^{2+}$. *J. Am. Chem. Soc.* **1998**, *120*, 8357−8365.
(25) Soda, T.; Kitagawa, Y.; Onishi, T.; Takano, Y.; Shigeta, Y.; Nagao, H.; Yoshioka, Y.; Yamaguchi, K. Ab initio computations of effective exchange integrals for H-H, H-He-H and Mn_2O_2 complex: comparison of broken-symmetry approaches. *Chem. Phys. Lett.* **2000**, *319*, 223−230.
(26) Illas, F.; de P. R. Moreira, I.; Bofill, J. M.; Filatov, M. Extent and limitations of density-functional theory in describing magnetic systems. *Phys. Rev. B: Condens. Matter Mater. Phys.* **2004**, *70*, 132414.
(27) de P. R. Moreira, I.; Illas, F.; Martin, R. L. Effect of Fock exchange on the electronic structure and magnetic coupling in NiO. *Phys. Rev. B: Condens. Matter Mater. Phys.* **2002**, *65*, 155102.
(28) Miralles, J.; Daudey, J.-P.; Caballol, R. Variational calculation of small energy differences. The singlet-triplet gap in $[Cu_2Cl_6]^{2-}$. *Chem. Phys. Lett.* **1992**, *198*, 555−562.
(29) Miralles, J.; Castell, O.; Caballol, R.; Malrieu, J.-P. Specific CI calculation of energy differences: Transition energies and bond energies. *Chem. Phys.* **1993**, *172*, 33−43.
(30) Andersson, K.; Malmqvist, P. Å.; Roos, B. O. Second-order perturbation theory with a complete active space self-consistent field reference function. *J. Chem. Phys.* **1992**, *96*, 1218−1219.
(31) Roos, B. O.; Andersson, K.; Fülscher, M. P. Towards an accurate molecular orbital theory for excited states: the benzene molecule. *Chem. Phys. Lett.* **1992**, *192*, 5−13.
(32) Krylov, A. I. Size-consistent wave functions for bond-breaking: the equation-of-motion spin-flip model. *Chem. Phys. Lett.* **2001**, *338*, 375−384.
(33) Krylov, A. I.; Sherrill, C. D. Perturbative corrections to the equation-of-motion spinflip self-consistent field model: Application to bond-breaking and equilibrium properties of diradicals. *J. Chem. Phys.* **2002**, *116*, 3194.
(34) Levchenko, S. V.; Krylov, A. I. Equation-of-motion spin-flip coupled-cluster model with single and double substitutions: Theory and application to cyclobutadiene. *J. Chem. Phys.* **2004**, *120*, 175−185.
(35) Bernard, Y. A.; Shao, Y.; Krylov, A. I. General formulation of spin-flip time-dependent density functional theory using non-collinear kernels: theory, implementation, and benchmarks. *J. Chem. Phys.* **2012**, *136*, 204103.
(36) Xu, X.; Gozem, S.; Olivucci, M.; Truhlar, D. G. Combined Self-Consistent-Field and Spin-Flip Tamm-Dancoff Density Functional Approach to Potential Energy Surfaces for Photochemistry. *J. Phys. Chem. Lett.* **2013**, *4*, 253−258.
(37) Zhekova, H.; Seth, M.; Ziegler, T. Introduction of a New Theory for the Calculation of Magnetic Coupling Based on Spin-Flip Constricted Variational Density Functional Theory. Application to Trinuclear Copper Complexes which Model the Native Intermediate in Multicopper Oxidases. *J. Chem. Theory Comput.* **2011**, *7*, 1858−1866.
(38) Krylov, A. I. Spin-flip configuration interaction: an electronic structure model that is both variational and size-consistent. *Chem. Phys. Lett.* **2001**, *350*, 522−530.
(39) Sears, J. S.; Sherrill, C. D.; Krylov, A. I. A spin-complete version of the spin-flip approach to bond breaking: What is the impact of obtaining spin eigenfunctions? *J. Chem. Phys.* **2003**, *118*, 9084−9094.
(40) Abraham, V.; Mayhall, N. J. Simple Rule To Predict Boundedness of Multiexciton States in Covalently Linked Singlet-Fission Dimers. *J. Phys. Chem. Lett.* **2017**, *8*, 5472−5478.
(41) Mayhall, N. J. From Model Hamiltonians to ab Initio Hamiltonians and Back Again: Using Single Excitation Quantum Chemistry Methods To Find Multiexciton States in Singlet Fission Materials. *J. Chem. Theory Comput.* **2016**, *12*, 4263−4273.
(42) Mayhall, N. J.; Head-Gordon, M. Computational Quantum Chemistry for Multiple-Site Heisenberg Spin Couplings Made Simple: Still Only One Spin-Flip Required. *J. Phys. Chem. Lett.* **2015**, *6*, 1982−1988.
(43) Mayhall, N. J.; Head-Gordon, M. Computational quantum chemistry for single Heisenberg spin couplings made simple: Just one spin flip required. *J. Chem. Phys.* **2014**, *141*, 134111.
(44) Stanton, J. F. On the vibronic level structure in the NO_3 radical. I. The ground electronic state. *J. Chem. Phys.* **2007**, *126*, 134309.
(45) Saeh, J. C.; Stanton, J. F. Application of an equation-of-motion coupled cluster method including higher-order corrections to potential energy surfaces of radicals. *J. Chem. Phys.* **1999**, *111*, 8275−8285.
(46) Stanton, J. F.; Gauss, J. Analytic energy derivatives for ionized states described by the equation-of-motion coupled cluster method. *J. Chem. Phys.* **1994**, *101*, 8938−8944.
(47) Nooijen, M.; Bartlett, R. J. Equation of motion coupled cluster method for electron attachment. *J. Chem. Phys.* **1995**, *102*, 3629−3647.
(48) Sattelmeyer, K. W.; Schaefer, H. F., III; Stanton, J. F. Use of 2h and 3h-p-like coupled-cluster Tamm-Dancoff approaches for the equilibrium properties of ozone. *Chem. Phys. Lett.* **2003**, *378*, 42−46.
(49) Wladyslawski, M.; Nooijen, M. In *The Photoelectron Spectrum of the NO_3 Radical Revisited: A Theoretical Investigation of Potential Energy Surfaces and Conical Intersections*; ACS Symposium Series; American Chemical Society: Washington, DC, 2002; Chapter 4, pp 65−92.
(50) Pieniazek, P. A.; Arnstein, S. A.; Bradforth, S. E.; Krylov, A. I.; Sherrill, C. D. Benchmark full configuration interaction model and equation-of-motion coupled-cluster model with single and double substitutions for ionized systems results for prototypical charge transfer systems: Noncovalent ionized dimers. *J. Chem. Phys.* **2007**, *127*, 164110.
(51) Pieniazek, P. A.; Bradforth, S. E.; Krylov, A. I. Charge localization and JahnTeller distortions in the benzene dimer cation. *J. Chem. Phys.* **2008**, *129*, 074104.
(52) Krylov, A. I. The Quantum Chemistry of Open-Shell Species. In *Reviews in Computational Chemistry*; Wiley, 2017; Vol. *30*, pp 151−224.
(53) Hsu, C.-P. The Electronic Couplings in Electron Transfer and Excitation Energy Transfer. *Acc. Chem. Res.* **2009**, *42*, 509−518.
(54) Casanova, D.; Head-Gordon, M. Restricted active space spin-flip configuration interaction approach: theory, implementation and examples. *Phys. Chem. Chem. Phys.* **2009**, *11*, 9779−9790.

DOI: 10.1021/acs.jctc.8b01268
J. Chem. Theory Comput. 2019, 15, 2278−2290

(55) Bell, F.; Zimmerman, P.; Casanova, D.; Goldey, M.; Head-Gordon, M. Restricted Active Space Spin-Flip (RAS-SF) with Arbitrary Number of Spin-Flips. *Phys. Chem. Chem. Phys.* **2013**, *15*, 358−366.
(56) Zimmerman, P. M.; Bell, F.; Goldey, M.; Bell, A. T.; Head-Gordon, M. Restricted active space spin-flip configuration interaction: Theory and examples for multiple spin flips with odd numbers of electrons. *J. Chem. Phys.* **2012**, *137*, 164110.
(57) Casanova, D. Avoided crossings, conical intersections, and low-lying excited states with a single reference method: the restricted active space spin-flip configuration interaction approach. *J. Chem. Phys.* **2012**, *137*, 084105.
(58) Casanova, D.; Head-Gordon, M. The spin-flip extended single excitation configuration interaction method. *J. Chem. Phys.* **2008**, *129*, 064104.
(59) Chien, A. D.; Zimmerman, P. M. Recovering dynamic correlation in spin flip configuration interaction through a difference dedicated approach. *J. Chem. Phys.* **2017**, *146*, 014103.
(60) Krylov, A. I. Equation-of-Motion Coupled-Cluster Methods for Open-Shell and Electronically Excited Species: The Hitchhiker's Guide to Fock Space. *Annu. Rev. Phys. Chem.* **2008**, *59*, 433−462.
(61) Smith, D. G. A.; et al. Psi4NumPy: An Interactive Quantum Chemistry Programming Environment for Reference Implementations and Rapid Development. *J. Chem. Theory Comput.* **2018**, *14*, 3504−3511.
(62) Turney, J. M.; et al. Psi4: an open-source *ab initio* electronic structure program. *WIREs Comput. Mol. Sci.* **2012**, *2*, 556−565.
(63) Dunning, T. H. Gaussian basis sets for use in correlated molecular calculations. I. The atoms boron through neon and hydrogen. *J. Chem. Phys.* **1989**, *90*, 1007−1023.
(64) Lofthus, A.; Krupenie, P. H. The spectrum of molecular nitrogen. *J. Phys. Chem. Ref. Data* **1977**, *6*, 113−307.
(65) Widmark, P.-O.; Malmqvist, P. Å.; Roos, B. O. Density matrix averaged atomic natural orbital (ANO) basis sets for correlated molecular wave functions. *Theor. Chim. Acta.* **1990**, *77*, 291−306.
(66) Carissan, Y.; Heully, J.-L.; Alary, F.; Daudey, J.-P. Calculation of the Ground and Excited States of a Mixed Valence Compound $[Fe_2(OH)_3(NH_3)_6]^{2+}$: A Class II or Class III Compound? *Inorg. Chem.* **2004**, *43*, 1411−1420.
(67) Carissan, Y.; Heully, J.-L.; Guihéry, N.; Alary, F. A study of the correlation effects upon the modelization of the double exchange phenomenon. *J. Chem. Phys.* **2004**, *121*, 9453−9460.
(68) Balabanov, N. B.; Peterson, K. A. Systematically convergent basis sets for transition metals. I. All-electron correlation consistent basis sets for the elements ScZn. *J. Chem. Phys.* **2005**, *123*, 064107.
(69) Lis, T.; Jezowska-Trzebiatowska, B. The Crystal and Molecular Structure of a New Type of Paramagnetic Binuclear Rhenium(IV) Compound, $Cs_3Re_2OCl_{10}$. *Acta Crystallogr., Sect. B: Struct. Crystallogr. Cryst. Chem.* **1976**, *B32*, 867−869.
(70) Hay, J. P.; Wadt, W. R. Ab initio effective core potentials for molecular calculations. Potentials for the transition metal atoms Sc to Hg. *J. Chem. Phys.* **1985**, *82*, 270−283.
(71) Woon, D. E.; Dunning, T. H. Gaussian basis sets for use in correlated molecular calculations. III. The atoms aluminum through argon. *J. Chem. Phys.* **1993**, *98*, 1358−1371.
(72) Campbell, J. R.; Clark, R. J. H. Resonance Raman, infra-red, and electronic spectral studies of the μ-oxo-decachlorodimetallate species, $[Re_2OCl_{10}]^{4-}$ and $[Re_2OCl_{10}]^{3-}$, and related ions. *Mol. Phys.* **1978**, *36*, 1133−1148.
(73) Ghosh, S.; Singh, S. K.; Tewary, S.; Rajaraman, G. Enhancing the double exchange interaction in a mixed valence V^{III}−V^{II} pair: a theoretical perspective. *Dalton Trans* **2013**, *42*, 16490−16493.
(74) Hehre, W. J.; Ditchfield, R.; Pople, J. A. Self-Consistent Molecular Orbital Methods. XII. Further Extensions of Gaussian-Type Basis Sets for Use in Molecular Orbital Studies of Organic Molecules. *J. Chem. Phys.* **1972**, *56*, 2257−2261.
(75) Rassolov, V. A.; Pople, J. A.; Ratner, M. A.; Windus, T. L. 6-31G* basis set for atoms K through Zn. *J. Chem. Phys.* **1998**, *109*, 1223−1229.

DOI: 10.1021/acs.jctc.8b01268
J. Chem. Theory Comput. 2019, 15, 2278−2290